Analytica Chimica Acta 1377 (2025) 344653

Contents lists available at ScienceDirect

Analytica Chimica Acta

journal homepage: www.elsevier.com/locate/aca

PHEMA polymer brush/Ag nanoparticle hybrids for SERS analytics: characterization and performance as versatile sensing substrate

Greta Peruzzi [a,*], Alessandro Ciccola [b,**], Francesca Costantini [b,c], Claudia Fasolato [d,e], Valentina Nigro [f], Cesare Manetti [b], Paolo Postorino [e], Gabriele Favero [b]

[a] Earth Sciences Department, Sapienza University of Rome, P.le Aldo Moro 5, 00185, Rome, Italy
[b] Environmental Biology Department, Sapienza University of Rome, P.le Aldo Moro 5, 00185, Rome, Italy
[c] Council for Agricultural Research and Economics, Research Centre for Plant Protection and Certification (CREA-DC), Via Carlo Giuseppe Bertero 22, 00156, Rome, Italy
[d] Institute for Complex Systems – National Research Council (ISC-CNR), P.le Aldo Moro 5, 00185, Rome, Italy
[e] Physics Department, Sapienza University of Rome, P.le Aldo Moro 5, 00185, Rome, Italy
[f] ENEA C.R. Frascati, Nuclear Department, Via Enrico Fermi 45, Frascati, 00044, Rome, Italy

HIGHLIGHTS

- Hybrid plasmonic polymer-based sensing platform.
- PHEMA brushes improve NPs stabilization and provide for a uniform, flexible alternative to traditional colloidal systems.
- Different synthetic routes employed to create six substrates with controlled NP size and brush thickness.
- SERS test of the platform on different probe molecules proved the wide range applicability with detection limits as low as 10^{-9} M.
- Broad applicability and integration potential with other analytical techniques (colorimetry or electrochemistry).

GRAPHICAL ABSTRACT

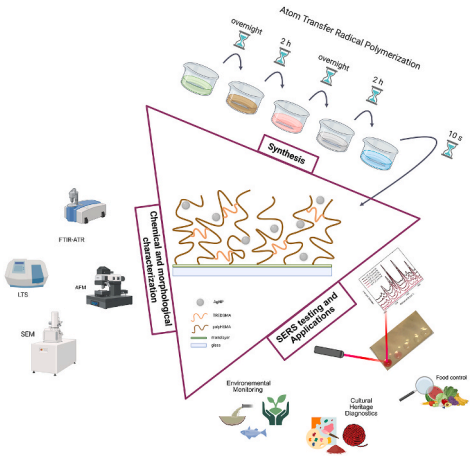

ARTICLE INFO

Handling Editor: Xiu-Ping Yan

Keywords:
Polymer brushes

ABSTRACT

Background: Surface plasmon resonance technology has shown broad applicability in different fields of molecular sensing. In particular, sensor arrays based on noble metal nanoparticles (NPs) have been demonstrated to be powerful tools for trace detection in food industry, environmental chemistry and Cultural Heritage conservation. The increasing demand for sustainable, uniform and flexible plasmonic platforms has led to introduce metal NPs

* Corresponding author.
** Corresponding author.
E-mail addresses: greta.peruzzi@uniroma1.it (G. Peruzzi), alessandro.ciccola@uniroma1.it (A. Ciccola), francesca.costantini@uniroma1.it (F. Costantini), claudia.fasolato@uniroma1.it (C. Fasolato), valentina.nigro@enea.it (V. Nigro), cesare.manetti@uniroma1.it (C. Manetti), paolo.postorino@roma1.infn.it (P. Postorino), gabriele.favero@uniroma1.it (G. Favero).

https://doi.org/10.1016/j.aca.2025.344653
Received 12 June 2025; Received in revised form 1 September 2025; Accepted 14 September 2025
Available online 15 September 2025

Plasmonic substrate
SERS
PHEMA
Sensing
AgNPs

into polymeric brushes, opening new perspectives for composite nanostructured materials and offering enhanced stabilization of NPs along with a defined spatial distribution.

Results: In this study, we report on the synthesis and characterization of a hybrid sensor system, comprising functionalized AgNPs anchored within a 2-hydroxyethyl methacrylate (PHEMA) polymeric brush, obtained through atom transfer radical polymerization. This polymer-based platform offers versatile applications – from sampling to detection – by leveraging the unique optoelectronic properties of a gel-brush network to achieve robust Surface Enhanced Raman Spectroscopy (SERS) performances. Different synthetic pathways were explored – occasionally using Triethylen Glycol Dimethacrylate as a crosslinker and varying the $AgNO_3$ reduction protocol. Six different substrates, with thickness ranging from 0.1 to 1 μm and NPs size between 20 and 200 nm were obtained and completely characterized through microscopic and spectroscopic analyses. SERS performances were tested for probe molecules (Rhodamine 6G, Malachite Green, Alizarin and Ochratoxin A), demonstrating the sensor potentiality for a low-concentration analyte detection across diverse matrices (down to 10^{-9} M), underscoring its applicability in a wide range of fields.

Significance and novelty: The PHEMA brush architecture offers enhanced control over SERS and acts as a stabilizer towards NPs, distinguishing it from traditional colloidal systems. The introduction of a new synthetic route for NPs reduction inside the polymer matrix – obtained by combining established methodologies for colloidal Ag preparation, – ensures an hybrid structure which is inherently compatible with other analytical techniques. These features significantly broadens the polymer-based system application scope and positions it as a flexible, multifunctional sensing interface.

1. Introduction

In recent years, novel advanced molecular sensing technologies have attracted substantial attention for practical applications in very diverse fields, from fundamental research questions to real-life analytical problems. Among these, surface plasmon resonance technology has undergone remarkable advancements, establishing itself as a versatile tool across diverse fields [1]. Its label-free detection capability, real-time monitoring, high precision, cost-effectiveness and low sample requirements have made it a keystone, opening the implementation of different analytical strategies for detecting analytes at trace concentrations in biomolecular sensing and biomedical applications [2,3], environmental monitoring [4,5], food safety [6,7] and cultural heritage diagnostics [8,9].

For instance, colorimetric sensors – made of gold or silver nanoparticles (NPs) – exploit Localized Surface Plasmon Resonance (LSPR) through analyte-induced NP aggregation, which results in detectable plasmonic shifts and colorimetric changes [10]. The use of plasmonic systems and NPs has also been exploited for the enhancement of fluorescence in various fluorescence-based analytical technologies [11–13]. Despite all these detection substrates being portable, user-friendly and sustainable, they provide limited to no structural information about the analytes, because of the detection methods exploited.

One effect, still based on LSPR, is Surface Enhanced Raman Scattering (SERS), which relies on the local enhancement of the Raman signal generated by metallic NPs, offering molecule-specific fingerprint signals. SERS spectroscopy, indeed, is denoted as one of the most advanced techniques for molecular sensing, combining exceptional sensitivity with chemical specificity, for a wide range of applications [14–19].

The sensitivity of SERS sensors is critically determined by the spectral profile of the LSPR, which is inherently influenced by the geometry, size, composition and arrangement of the plasmonic NPs [1,14]. To date, various types of SERS substrates have been reported, including rough metallic surfaces [20], nanomaterials with unique morphologies [21,22], and hybrid composites [23,24]. To maximize the electromagnetic near field enhancement, it is particularly advantageous to engineer the so-called “hotspots”, e.g. apexes, crevices or interparticle gaps within a NP aggregate. Very high enhancements are achievable through lithography [25–28] and other nano-fabrication methodologies [29,30], usually characterized by good reproducibility in the achieved SERS signal enhancement. The use of templates with periodic porous structures for the deposition of Ag or Au NPs represents a promising strategy for the fabrication of high-performance SERS substrates [31–33]. However, it is important to remark that these techniques often require high precision control, so their actuation is time-consuming and, in some cases, quite expensive for the large scale production.

Colloidal plasmonic NPs can be employed as highly sensitive SERS substrates. Beside the sensitivity, their great advantage is the easy production through rather simple chemical synthetic routes. From this point of view, a main aspect to be evidenced is the wide choice of protocols available in the literature [34–37], which allow a fine tuning of the desired features of achievable NPs, especially in the case of Ag based ones, granting an improved plasmon efficiency at a lower material cost compared to Au [38]. Unfortunately, these AgNPs are also characterized by an intrinsically low stability, both chemical – in terms of oxidation susceptibility [39] and physical – as their colloidal stability can be perturbed because of the dispersion high ionic strength, leading to irreversible NP aggregation. Furthermore, the SERS signal enhancement in these systems is produced by the interparticle hotspots, resulting in poor reproducibility when it derives from uncontrolled NP aggregation, both in liquid and on solid substrates, where NP clustering gives rise to the so-called coffee ring effect, dramatically affecting the signal enhancement reproducibility. That poses some crucial issues towards applications. To solve this problem, Cong and colleagues have proposed the use of hydrogel microbeads as a scaffold to “freeze” the NPs in a 3D network, producing a high-yield, uniformly dispersed and SERS active biosensor [40].

The increased demand for high performance sensors has pointed out polymer-based composites as alternative systems with great potential [41]. Recent innovations have introduced polymer brush-based [42–44] platforms as promising solutions for enhancing the stability, uniformity and sustainability of SERS substrates [45–49]. Polymer brushes are nanoscale-macromolecular structures achievable from various typologies of monomers, grafted by one end to a surface. Their structure allows for the immobilization of several types functional molecules such as enzymes, aptamers, proteins and inorganic particles [50–54]. Moreover, according to the synthetic routes adopted, their organization in different 3D structures can be finely tuned, from mono-layers to extended networks, with an increase in the amount of groups available to bind the functional molecules. The control over the polymeric chain growth is an advantage, not only for the macromolecule organization, but also for their potential use to embed metal NPs with defined features, such as size and shape [55–57]. Due to their phase transition properties and ability to control the spacing between NPs, these polymer structures enable controlled and high-density hotspot generation, thus improving the SERS detection efficiency and reliability [42,55]. Moreover, their combination with metal NPs results in a strong stabilization of the latter, protected from atmospheric oxidation, thus conferring a higher robustness for analytical performances [39]. This represents a crucial

step towards the effective technology transfer of SERS into routine analytics, granting its large scale use in place of more sophisticated methods. The exploitation of polymer engineering and its effect on optimizing NP size, shape and composition, paves the way for a new generation of highly customizable plasmonic sensors, tailored for advanced applications.

In this study we investigate the effect of stabilizing AgNPs, synthesized according to different simple protocols reported in the literature, by means of polymer brushes based on poly (2-hydroxyethyl methacrylate) (PHEMA), for SERS analytical applications. The monomer was selected with reference to several features, which grant a remarkable versatility. Firstly, PHEMA is highly compatible with on-site reduction protocols of metals, resulting in a scaffold network for NP anchoring and growth. PHEMA polymerization can be finely addressed to achieve different 2D or 3D polymeric structures [55,58], which are generally resistant to pH and temperature changes; however, these properties are finely tunable for specific applications, just by introducing specific monomers for copolymerization [59]. Finally, PHEMA presents a general affinity for entrapping and adsorbing different types of compounds – e.g., dyes, drugs, and biological compounds, which represent a potential strategy for improving the detectability of different analytes by SERS [60]. Given these advantages, we tested two different protocols for producing PHEMA polymer brushes – with and without a cross-linker (Triethylene Glycol Dimethacrylate; TREDGMA) – in combination with three different protocols of silver NPs reduction. The achieved AgNPs-loaded polymer brushes were characterized by means of different microscopic (Scanning Electron Microscopy, SEM; Atomic Force Microscopy, AFM) and spectroscopic (Fourier Transformed Infra-Red, FT-IR, in Attenuated Total Reflectance, ATR; Light Transmission Spectroscopy, LTS) techniques, and the SERS performance were evaluated for the quantitative detection of different molecules of interest in several fields, such as: Malachite Green, a synthetic water soluble dye, which is a carcinogenic pollutant deriving from textile wastewaters and biopesticide industry [22,61]; Alizarin, one of the main anthraquinone chromophores of madder, a natural dyestuff historically used to dye textile and prepare lake pigments [62,63]; Ochratoxin A, a mycotoxin produced by some species of Fungi, which is commonly found in food and beverages and it is highly toxic for human health [64,65].

2. Experimental section

2.1. Materials and characterization

All reagents were purchased from Sigma-Aldrich Chemicals and used without any further purification. 2-bromo-2-methyl-propionic acid 3-trichlorosylanylpropyl ester was synthesized following a reported procedure [66]. Ethanol (analytical reagent grade) was used without further purification, while toluene was distilled over sodium. Water was purified with a Milli-Q pulse (MILLIPORE, R = 18.2 MΩ cm) ultra-pure water system. Glass slides from Anchor (China National Machinery Imp. & Exp. Corp. Jiangsu Branch) were purchased and cut in half for desired length. Rhodamine 6G, Malachite Green, Alizarin and Ochratoxin A were purchased as standards from Sigma Aldrich.

FTIR spectra were acquired using a Bruker Alpha II spectrometer coupled to a diamond cell ATR accessory. For each substrate, three spectra were acquired in different areas. For each spectrum, 40 scans with a resolution of 4 cm^{-1} were collected. With reference to their high reproducibility, the three spectra for each substrate were averaged to compare spectra obtained from different substrates.

LTS measurements were performed using a custom setup composed of a Laser-Driven Light Source, a Czerny-Turner spectrometer with cylindrical optics and a CMOS camera. Spectra were acquired in the range 400–800 nm to investigate the plasmonic resonance properties of the NPs formed in the polymer brushes. Four spectra were acquired for each sample, two on the front and two on the back of the sensor. Since substrates are quite homogeneous and there is no difference in the spectral shape between the two sets of measurements for each sample, data were averaged. Also, spectra of glass and polymer were subtracted for the background.

SEM measurements were performed using the HR-FESEM (Field Emission Scanning Electron Microscopy), AURIGA Zeiss model. Images were acquired at different magnifications in both backscattered and secondary electron modes. No metallization on samples was performed, while conductivity was granted through a copper filament bridging the samples to the stub.

AFM measurements were performed using the A100 PLUS AFM (A.P.E. Research s.r.l., Area Science Park, Basovizza (TS), Italy) operating in non-contact mode. All images were taken in air ambient conditions, with commercial MikroMasch cantilevers HQ:NSC15 (nominal force constant from 20 to 80 N/m and resonance frequency from 265 to 410 kHz) on two different size areas (5 × 5 μm^2 and 2.5 × 2.5 μm^2). Measurements of film thickness were performed by measuring the step profiles over a 50 × 50 μm^2 area across the scratches made on the sample surface in three different regions. For data analysis the open-source software Gwyddion was used. Root Mean Square roughness (Sq), defined as the standard deviation of the distribution of surface heights, was measured for characterizing the surface roughness.

To test the SERS performances of the obtained substrates, Rhodamine 6G (Rh6G) was selected as a probe molecule, with reference to the literature [33], to evaluate the reproducibility and the enhancement factor of the substrate. Different concentration solutions – ranging from 10^{-7} M to 10^{-3} M – were deposited on the substrate and let dry; Raman spectra were acquired in correspondence using a Horiba Jobin-Yvon HR-Evolution coupled with a microscope with interchangeable objectives and equipped with lasers at both 633 nm and 532 nm wavelength. To evaluate the reproducibility of the Raman signal, analysis was performed in Raman mapping mode, collecting 81 spectra for every concentration standard in an area of 27 × 27 μm^2. For the first trials, Raman spectra were acquired with the 633 nm laser in two ranges of interest: 50-1200 cm^{-1} and 1050-2000 cm^{-1}. After a preliminary evaluation of the main signals of Rh6G, Raman maps were acquired only in the range 650–1800 cm^{-1}, right after polymer synthesis and after one month. In order to assess the relationship between the Raman signal and the concentration of Rh6G, for every concentration the map spectra were averaged and processed (polynomial fit and background subtraction were performed using the software LabSpec6). Areas of some selected peaks in the averaged spectrum – obtained from peak-fitting deconvolution of Gaussian and Lorentzian curves – were integrated and used to build the calibration curves, through the software Origin 2018 (®OriginLab) and the available tools. The calibrations curves were compared in terms of slope, to establish the main peaks to use for the quantification. Moreover, the limits of detection were estimated from the same curves. The SERS enhancement factor was evaluated by comparison of the acquired SERS spectra with the standard Raman spectra collected, for Rh6G solution at 10^{-3} M, on a blank substrate, obtained by synthesis of the polymer brushes with no reduction of silver and consequent absence of silver nanoparticles. The enhancement factors were calculated in two different ways, based on the highest (10^{-3} M) and lowest concentration of Rh6G detectable for every substrate, to obtain an estimation of the enhancement at different concentrations. The following equation was used to calculate the EF:

$$EF = \left(I_{-SERS} \cdot C_{-Raman}\right) / \left(C_{-SERS} . I_{-Raman}\right)$$

where I_{SERS} is the area of a selected reference peak for the SERS spectrum, C_{SERS} is the concentration of the Rh6G solution used for the SERS experiment, C_{Raman} is the concentration of the Rh6G solution used for Raman and I_{Raman} is the area of the same reference peak for the Raman spectrum. Regarding the calculation methods, in Method_1 C_{SERS} was equal to C_{Raman}, while in Method_2 the lowest integrable concentration was used for C_{SERS} and the highest concentration was used for C_{Raman}.

Subsequently, SERS spectra of lower concentration of Rh6G solution

were acquired with the 532 nm laser for the most promising substrate, evaluated on the basis of previous analyses. Analysis was performed again in Raman mapping mode, collecting 81 spectra for every concentration standard in an area of 27 × 27 μm^2, for solutions ranging from 10^{-9} M to 10^{-5} M. Spectral processing was performed through LabSpec6 software, while peak fitting and calibration curve building were performed through Origin 2018, analogously to the procedure used for the red laser.

Solution of Malachite Green in water, were prepared in the concentration range 10^{-5} – 10^{-10} M; Alizarin and Ochratoxin A solutions were prepared in the same range of concentrations, but in ethanol and acetonitrile, respectively. All three analytes were analyzed using the red laser in the region of their respective fingerprint.

2.2. Synthesis of the substrates

The synthesis of the trial substrates was carried out following published procedures [55,56]. Briefly, glass slides were first cleaned with a Piranha solution (H_2SO_4:H_2O_2, 3:1) and then copiously rinsed with water and dried with a stream of nitrogen. (Caution: Piranha solution is a very strong oxidant and reacts violently with many organic materials). Glass slides were then soaked in a solution of 2-bromo-2-methyl-propionic acid 3-trichlorosylanylpropyl ester (20 μL) in dry toluene overnight under argon. After, glass slides were rinsed with dry toluene and, eventually, with acetone to remove excess of reaction, and dried with a stream of nitrogen.

A solution of PHEMA in water was degassed by bubbling through dry nitrogen for 30 min, at times adding 2 % of TREDGMA. Indeed, the synthesis of polymer brushes was accomplished for two different batches: one in the presence of the TREDGMA crosslinker and the other in absence of it. The following steps of reaction were the same for the two batches. CuCl (28 mM), $CuBr_2$ (8 mM) and 2,2′-bipyrydyl (78 mM) were added to the solution to dissolve all solids; the mixture was then stirred for 10 min under flow of argon until yielded a dark brown solution. Afterwards, the initiator-coated glass slide was placed in a flask sealed with a septum that was filled with argon; the monomer solution was syringed inside the flask. The glass slide was left in contact with the solution for 2 h. After the polymerization, the substrates were rinsed with ethanol and dried with a stream of nitrogen. The PHEMA and PHEMA-TREDGMA polymer films were treated with a solution of succinic anhydride and triethylamine in dry tetrahydrofuran. Subsequently, they were rinsed with ethanol and dried with a stream of nitrogen. Finally, the substrates were first kept in a solution of $AgNO_3$ (either 1 mM or 50 mM, see Table 1) for 2h and then soaked in a reducing solution for the production of AgNPs. About this step, three different protocols – whose synthetic routes are summarized in Table 1 – were tested, using either sodium borohydride [56] or hydroxylamine hydrochloride [34] as reducing agents. The different routes were compared in terms of morphology and size distribution of NPs, while the effect of varying the contact time between substrates and reducing solutions was also evaluated.

Table 1
Details of the different synthetic paths followed to produce the six polymer brushes substrates. For the sake of completeness, polymer brushes samples without NPs are also shown.

Sample name	Synthetic path
s_H	Polymer brushes grafted from PHEMA (H) without crosslinker
s_H_B	Polymer brushes grafted from PHEMA (H) without crosslinker, NPs produced reducing $AgNO_3$ 50 mM using $NaBH_4$ 1.3 mM (B) [56]
s_H_L	Polymer brushes grafted from PHEMA (H) without crosslinker, NPs produced reducing $AgNO_3$ 1 mM using NH_2OH ·HCl 3 mM (L) [34]
s_H_H	Polymer brushes grafted from PHEMA (H) without crosslinker, NPs produced reducing $AgNO_3$ 50 mM using NH_2OH ·HCl 75 mM (H)
s_HT	Polymer brushes grafted from PHEMA (H) and TREDGMA (T)
s_HT_B	Polymer brushes grafted from PHEMA (H) and TREDGMA (T), NPs produced reducing $AgNO_3$ 50 mM using $NaBH_4$ 1.3 mM (B) [56]
s_HT_L	Polymer brushes grafted from PHEMA (H) and TREDGMA (T), NPs produced reducing $AgNO_3$ 1 mM using NH_2OH ·HCl 3 mM (L) [34]
s_HT_H	Polymer brushes grafted from PHEMA (H) and TREDGMA (T), NPs produced reducing $AgNO_3$ 50 mM using NH_2OH · HCl 75 mM (H)

3. Results and discussion

3.1. Characterization of the polymer brushes

The synthesis of the NP-loaded polymer brushes on glass was conducted as described in the Experimental section. Two different protocols for the production of brushes were followed (presence or absence of the TREDGMA crosslinker) and three different methods for AgNP reduction inside the polymer structure were tested (using sodium borohydride or hydroxylamine hydrochloride as reducing agents in different concentrations). The modification of the synthetic path led to the production of six different substrates (Table 1) which resulted in optically homogeneous upon visual inspection. Their homogeneity was confirmed through chemical and morphological characterization.

3.2. Spectroscopic characterization

The AgNP-loaded and pristine polymer brushes were chemically characterized in order to evaluate the reaction outcome and polymer grafting on the glass substrate. First, FTIR spectroscopy in ATR mode was performed. The acquired spectra confirmed the reaction success and a comparison with literature data proved the effective grafting of the polymer on the glass substrate [55,56]. In particular, as reported in A1 (Supplementary Material, SM), FTIR peaks at 2875, 2933, 2958 and 2988 cm^{-1} are indicative of the C–H stretching modes of methylene and methyl groups of PHEMA, whilst peaks at 1720-1725 cm^{-1} are attributed to the carbonyl group moieties of PHEMA after the reaction with succinic anhydride. A peak at 1570 cm^{-1} is clearly observable, with high intensity, in the final substrates: this band can be attributed to the interaction between carboxylate groups and silver, highlighting the formation of NPs on and inside the polymer brushes [56]. FTIR spectra highlighted a major difference between films obtained without TREDGMA and their analogues obtained including it as crosslinker: in the latter case, spectral features of glass are more prominent in the FTIR spectra of final substrates, suggesting a lower thickness of the polymer brushes in comparison with the other set of samples. This suggests the possibility to control the production of the substrates and their thickness by simply varying the concentration of the crosslinker, a fundamental factor for the control of surface interaction with analytes.

LTS measurements were carried out on the substrate and allowed identifying the spectral signature associated with the LSPR, confirming the formation of metal NPs. Moreover, the LSPR spectral shape suggested a smaller size of NPs for samples obtained in presence of crosslinker, while in the crosslinker-free samples the NPs are larger in size or tend to form bigger aggregates. In Fig. 1, we show the LTS spectra of samples obtained in absence or presence of the crosslinker. sHT_B and sHT_L samples (Fig. 1b) exhibit a plasmonic peak around 400 nm, which is characteristic of isolated AgNPs [67]. In contrast, sample sHT_H features a plasmonic extinction peak at a shorter wavelength, still indicative of single NPs but smaller in size. On the other hand, the LTS spectra of samples synthesized without TREDGMA (Fig. 1a) show plasmonic features typical of AgNP aggregates [38]. For instance, sample sH_H is characterized by an extinction peak around 600 nm, suggesting the presence of dimers or larger aggregates. These observations support the hypothesis that the use of a crosslinker, and the consequent formation of a structured network, influences the growth and aggregation of metal NPs.

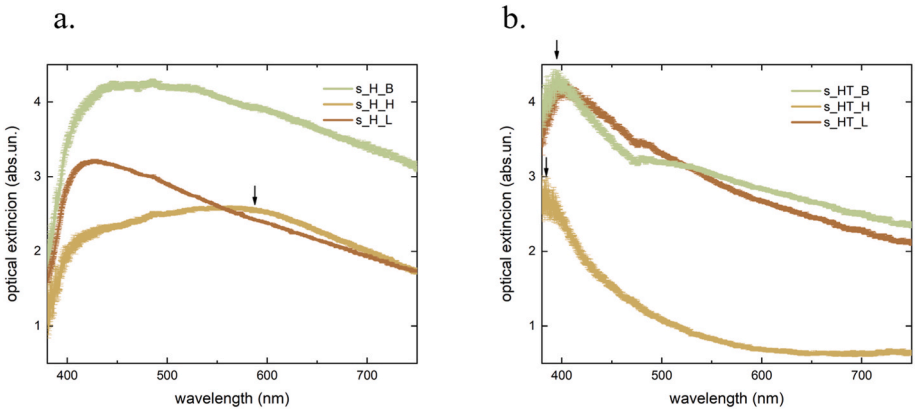

Fig. 1. LTS spectra showing optical extinction of plasmonic structures in: (a) substrates produced in absence and (b) presence of the TEDGMA crosslinker.

3.3. Morphology of the substrates and NPs distribution

SEM and AFM analyses were performed to obtain information about substrate morphology, NP size and spatial distribution. From SEM measurements, it was possible to assess both the surface appearance of the polymer film and the NP size, confirming the information obtained by previous LTS analyses. In Fig. 2, the comparison of the two polymer films without NPs is provided. About the substrate obtained in the absence of TREDGMA (s_H; Fig. 2a), a brush-like regime conformation occurs at high grafting density [68]. In contrast, the presence of the cross-linker promotes the formation of pillar-like structures (s_HT; Fig. 2b), likely due to the aggregation of polymer chains interconnected by TREDGMA between individual monomers. The morphological characteristics of these polymers – either the formation of pillars or not – is likely to deeply influence the formation of NPs and aggregates (Fig. A2 and SM). This difference can be truly appreciated by comparing the two sample batches: in crosslinker-free polymers, the absence of TREDGMA leads to the formation of bigger aggregates because of the brushes' stabilization features which are not effective. In this set of samples, NPs tend to aggregate, similarly to what happens in colloidal suspensions, as they have more space to interact within the polymer chains. The crosslinker, instead, acts as a template and the presence of pillars determines smaller NPs with a more patterned distribution. As clear from Fig. 3a, b, c, in crosslinker-free samples s_H_B, s_H_H and s_H_L, large NP aggregates of variable size are observed all over the surface. In some areas, they reach dimensions of several hundred nanometers and the morphological features and the dimensions of single NPs are difficult to distinguish. In particular, sample s_H_B presents a "rug-like" dense morphology, where single NPs are barely visible (Fig. 3a). Likewise, sample s_H_H (Fig. 3b) displays a jagged morphology with dense aggregates, which also obscures the identification of single NPs. Finally, in sample s_H_L (Fig. 3c), individual NPs are either embedded in or completely obscured by amorphous, liquid-like structures [69] with dimensions in a range between 100 and 300 nm. Based on their morphological features, these structures may be evidence of salt residues – most probably hydroxylamine hydrochloride or other Cl salts (NaCl or AgCl) – formed as by-products of NPs synthesis within the polymer film during $AgNO_3$ reduction process.

On the contrary, the addition of TREDGMA and the consequent organization in crosslinked brushes provides greater stability, influencing NP growth and organization. However, the morphological characteristics of cross-linked polymer films and, consequently, the pillar-like features, can be influenced by the reduction pathway adopted for NP production. For example, in Fig. 3e and f, SEM images for samples s_HT_H and s_HT_L show different polymer morphological features compared to the pillar-like structures observed in Fig. 2b. In the case of sample s_HT_H (Fig. 3e), pillars appear deformed, showing reduced regularity; in sample s_HT_L (Fig. 3f) pillars are more scattered and less prominent. This behavior is plausibly associated with the reduction pathway: although both AgNP-polymer composites reduction protocols are based on the same reagents (hydroxylamine hydrochloride and NaOH), the concentrations differ by an order of magnitude (see Table 1 in Experimental Section). In particular, the higher concentrations in the "H" reduction method are expected to strongly influence the morphology of the polymeric film and consequently the nanostructure morphologies. Nevertheless, the mechanism behind these alterations cannot yet be fully identified and further investigations will be required to clarify the role of reaction conditions on structural changes. On the other hand, in sample s_HT_B (Fig. 3d), where the reduction pathway is once again different (use of $NaBH_4$ as reducing agent), pillars do not seem to show any particular difference with the blank substrate and the pillar-like structure are roundish and well organized.

As TREDGMA acts as a template for NPs, in all cross-linked samples, they are present in small and regular clusters, homogeneously

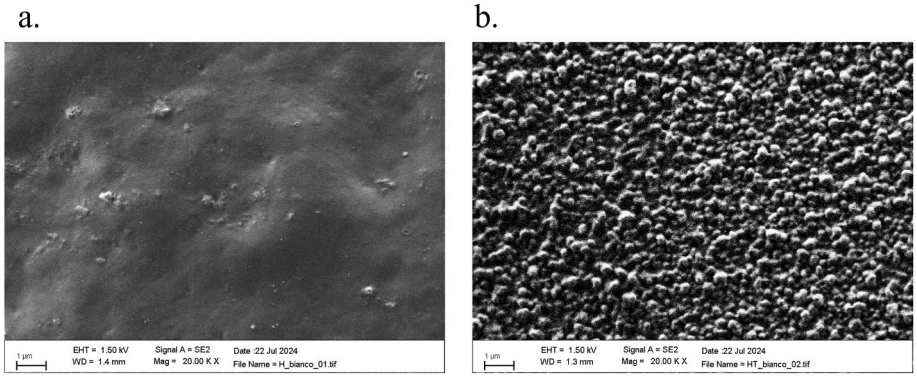

Fig. 2. SEM image of PHEMA polymer brushes grafted in absence (a) or presence (b) of the TREDGMA crosslinker.

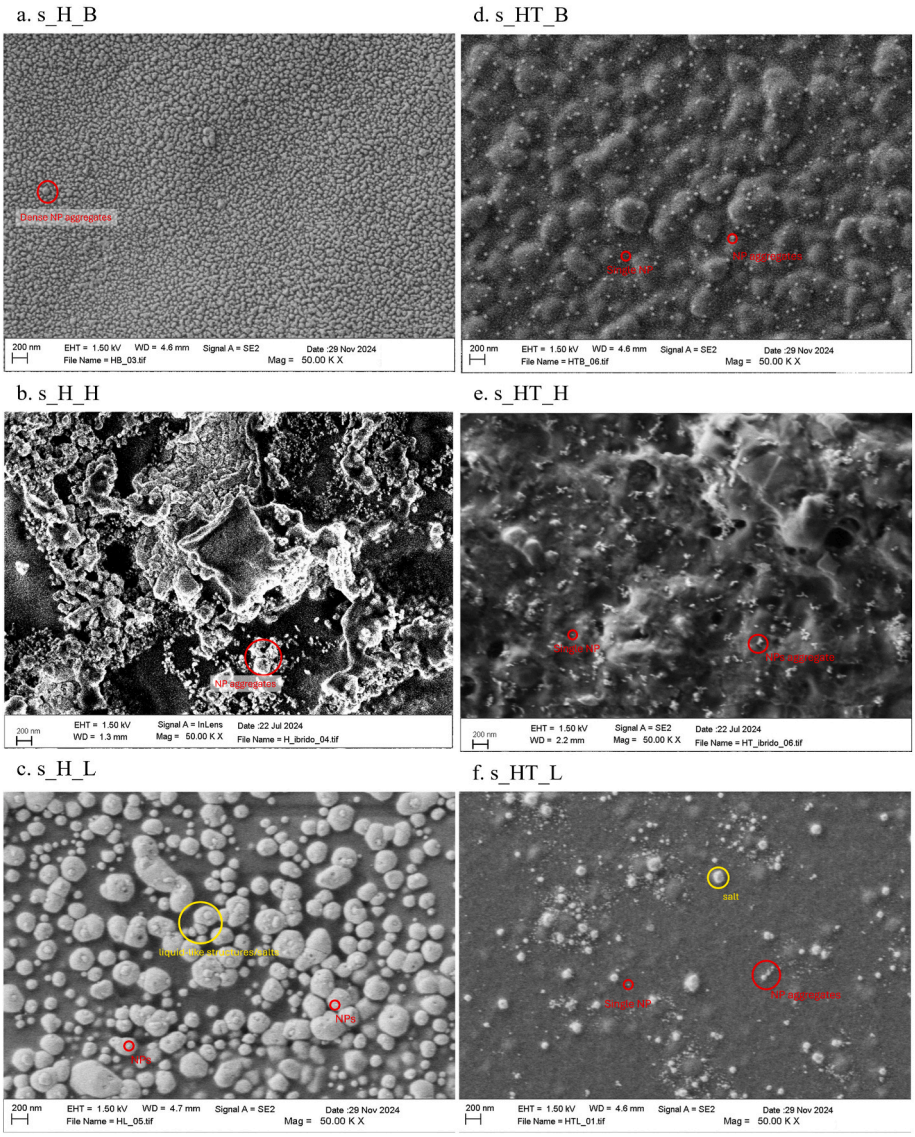

Fig. 3. SEM images of the six samples, according to the legend above.

distributed all over the polymer brushes with well-defined edges, maintaining their shape and size within the aggregates. In particular, in samples s_HT_H and s_HT_L, (Fig. 3e and f), NPs have size between 20 and 70 nm while, for sample s_HT_B (Fig. 3d), NP dimensions are even below 20 nm. Moreover, in sample s_HT_B, some structure with the typical salt-like shape and dimension around 50 nm can be observed (Fig. A3 and SM), which can be attributed to $NaBH_4$ residues due to the method of production of NPs (excess of reaction). Similarly, in sample

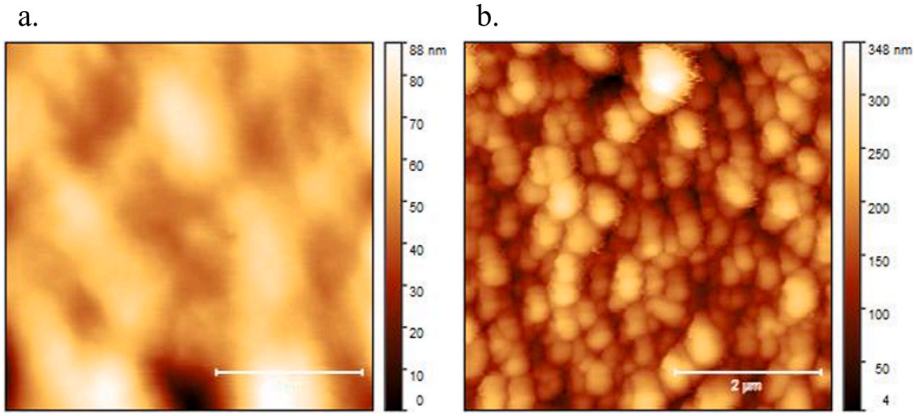

Fig. 4. AFM images on a 5 × 5 μm^2 area of samples s_H (a), s_HT (b). Scale bar: 2 µm.

s_HT_L (Fig. 3f) some structures approximately 100 nm in size are visible, which could once again be attributed to salt residues. Regardless, it is important to underline that the hypothesis of salt presence is based solely on morphological differences. More accurate elemental analysis (such as EDX, XRD or XPS) would be required to unambiguously determine the elemental nature of these structures.

AFM data confirmed the observation already noted from SEM images. In particular, Fig. 4 clearly shows the different morphologies of samples in the absence (s_H) or presence (s_HT) of the crosslinker: the first has a smooth surface, with a Root Mean Square (RMS) roughness $S_q = 11.0 \pm 0.5$ nm, where no particular organization is visible (Fig. 4a); on the contrary Fig. 4b highlights the presence of some pillar-like structures in the s_HT blank substrate with dimensions around 300 nm and a RMS roughness $S_q = 43 \pm 5$ nm. For the samples obtained without the cross-linker (s_H_B, s_H_H, s_H_L), AFM data do not allow clearly identifying either isolated NPs nor small aggregates. However, in samples s_H_H and s_H_L (Fig. 5b and c), nanostructures with size around 100 nm can be ascribed to the presence of large NPs. On the contrary, single NPs can be more easily identified in samples prepared by adding the cross-linker (s_HT_B, s_HT_H, s_HT_L), as shown in Fig. 5c,d,e. In particular, in samples s_HT_B and s_HT_L (Fig. 5d–f), single NPs with size around 30 nm are observed, while in hybrid substrates s_HT_H, NPs are more specifically grouped in clusters (Fig. 5e). These results confirm that the presence of TREDGMA – and the consequent formation of pillar-like structures – acts indeed as a template for NP size growth and distribution: NPs are larger in substrates without the cross-linker compared to those obtained with the cross-linked polymers.

AFM measurements also permitted the evaluation of the polymer brush thickness (*t*): cross-linked films appeared thinner than those obtained in the absence of TREDGMA, confirming ATR data. For instance, in all the samples obtained with HEMA and TREDGMA *t* is on the order of 100–200 nm, whilst PHEMA substrates show thicknesses one order of magnitude greater than their counterparts.

3.4. Evaluation of the platform as SERS substrate

3.4.1. Tests on Rhodamine 6G

After the characterization, SERS performances of the substrates were

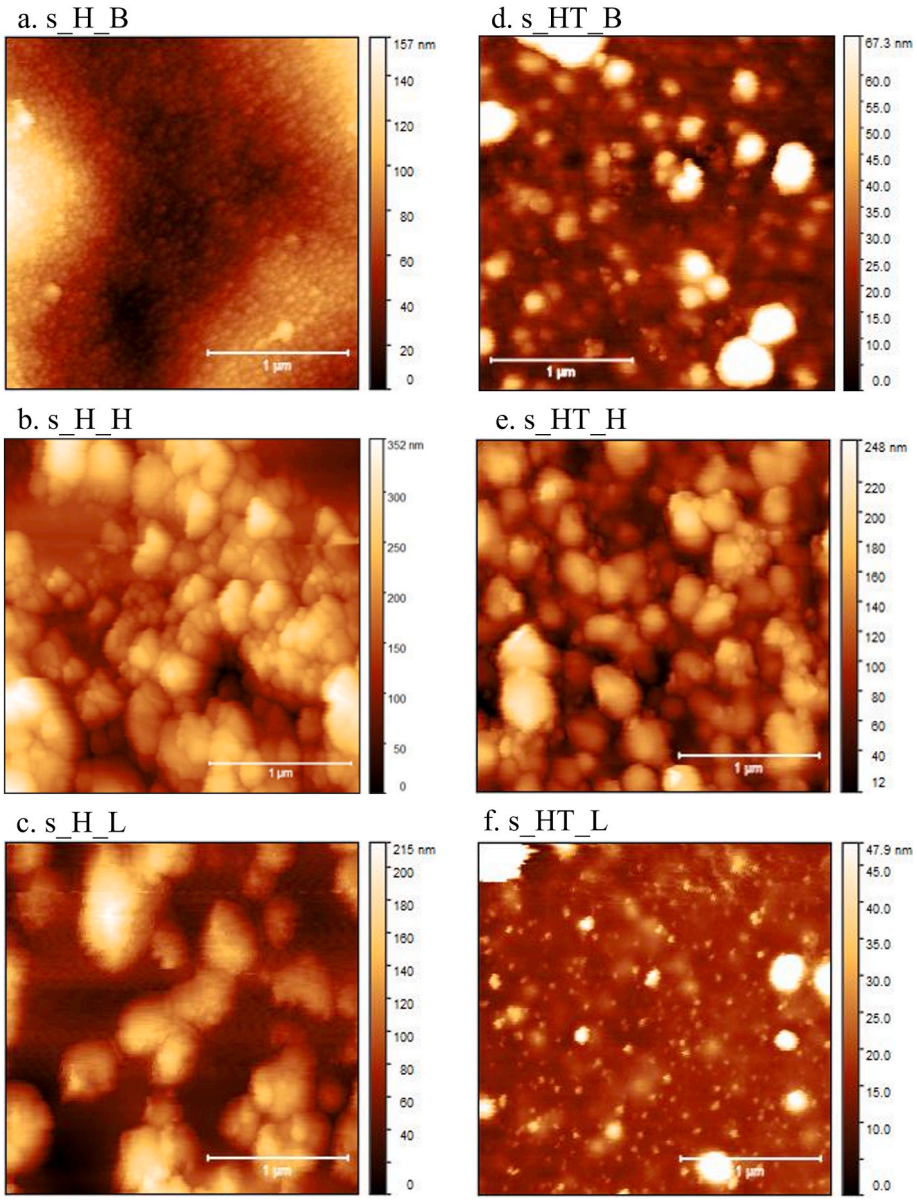

Fig. 5. AFM images on a 2.5 × 2.5 µm^2 area of samples s _H_B (a), s_H_H (b), s_H_L (c), s_HT_B (d), s_HT_H (e), s_HT_L (f). Scale bar: 1 µm.

evaluated in terms of reproducibility and enhancement factor. With reference to the literature [33,70], Rhodamine 6G (Rh6G) was selected for this purpose as a probe. For the first set of measurements, a 633 nm laser was used to perform analyses, to avoid electronic resonance conditions for Rh6G [71]: this allows estimating the actual signal amplification attributable only to the SERS phenomenon, with no positive contribution coming from Resonance Raman [72]. Preliminary measurements were focused on establishing a methodology for the evaluation of the SERS enhancement, comparing signals obtained with the standard Raman spectrum of Rh6G acquired on the analogue substrate without AgNPs (Fig. 6a). The evaluation of SERS performance was then performed for all the substrates.

The most intense SERS bands of Rh6G were observed at 1313 cm^{-1} (C–*O*–C stretching vibration), 1363 cm^{-1}, 1510 cm^{-1} and 1650 cm^{-1} (C–C stretching) [33,73]. They were selected to build quantification curves by correlating the area of this signal and the concentrations of tested solutions. Overall, we obtained linear quantification curves for all the peaks selected (Fig. A4 and SM). For SERS enhancement studies, the area of peak 1510 cm^{-1} was used, because of the higher slope of the calibration curve, allowing comparison of the different substrates applicability. Fig. 6c shows the linear dependency between the logarithm of standard concentration in the tested range and the area of 1510 cm^{-1} peak, estimated through peak fitting deconvolution and registered for different substrates. Quantification curves for samples s_H_B, s_H_H, s_H_L (dotted plots in Fig. 6c) exhibit a higher slope which reflects and confirms the results of the morphological characterization: in the absence of crosslinker, NPs lack a structural template, are grouped in bigger aggregates and exhibit a broader distribution with substantial gaps between them (Fig. A5 and SM). The presence of a large number of big aggregates facilitates the formation of highly intense hotspots due to NP size [74] that are capable of strong signal intensity enhancement. As the Rh6G concentration increases, the probability of molecules of being located near an hotspot also increases, leading to a sudden enhancement of the signal (hence higher slopes of the intensities vs concentration trend). In particular, s_H_H presents the highest slope, associated with the highest intensities, in particular at higher concentrations (Fig. 6c). This is also coherent with the spectral shape of the LSPR in Fig. 1a, predicting an optimized enhancement at the laser wavelength (633 nm) for this sample. However, the crosslinker-free configuration exhibits a lower reproducibility, as evidenced by the irregular trends for the fitted curves (e.g., sample s_H_L in Fig. 6c). On the other hand, when TREDGMA is incorporated into the polymer (samples s_HT_B, s_HT_H, s_HT_L), NP spacing and templating are established. This results in smaller NPs but a higher density of hotspots, as the interparticle distance is reduced by the presence of the crosslinker and NPs are homogeneously distributed either as single NPs or in clusters (Fig. 3). This arrangement not only produces a more reproducible signal, but also enables the detection at lower analyte concentrations, since the probability of having molecules being located near an hotspot is increased, thereby the Limit of Detection (LOD) is lowered to values below 10^{-6} M as in sample s_HT_H (Fig. 6c).

Moreover, the comparison between standard Raman spectra obtained for Rh6G 10^{-3} M solution on the polymer brushes without AgNPs and the SERS analogues from the NPs-loaded films allowed the estimation of the enhancement factor (EF) that was calculated in two different ways (cfr. Experimental section) and listed in Table 2 for all the substrates. Note that for the EF calculation, the ratio between the SERS and Raman intensities was calculated by conducting the same experiment on the polymer substrate with and without the plasmonic nanoparticles. SERS and Raman intensities were normalized to the nominal concentration used for each experiment and, in order to foster an unbiased analysis of the results, no considerations were made on the influence of the plasmonic particles on the depth of the scattering volume. That implies the figures resulting from the calculations are significantly smaller than those obtained in other cases, were different calculation methods for the EF were implemented [38]. Again, the best results were obtained for s_HT_H substrate: it represents the most promising substrate for analyte detection with reference to the validation criteria for analytical application featuring the highest EF (around 4 orders of magnitude) and the lowest LOD, representing a better choice to push its application for trace detection.

The final evaluation of SERS performances was carried out using a 532 nm laser, in agreement with literature [33], to compare the selected substrate with other established SERS-based methods. The use of a green laser added further enhancement effect, due to the resonant Raman features of Rh6G, enabling further improvement of the analytical performances and allowing detection at lower concentrations (Fig. 7a). Indeed, Raman bands of the probe molecule are now clearly visible until 10^{-7} M and still integrable at 10^{-9} M, bridging the LOD below this concentration (Fig. 7b). The EF was calculated by comparing standard Raman spectra obtained for Rh6G 10^{-5} M solution on the polymer brushes without AgNPs and the SERS analogues from the NPs-loaded hybrid films analogous to previous data. The result was around 10^5.

Table 2
Enhancement factors calculated for all six samples on data acquired with the 633 nm laser.

Sample	EF (method 1)	EF (method 2)
s_H_B	~10^2	~10^3
s_H_L	~10^2	~10^2
s_H_L	~10^2	~10^3
s_HT_B	~10^3	~10^3
s_HT_L	~3*10	~10^2
s_HT_H	~10^4	~10^4

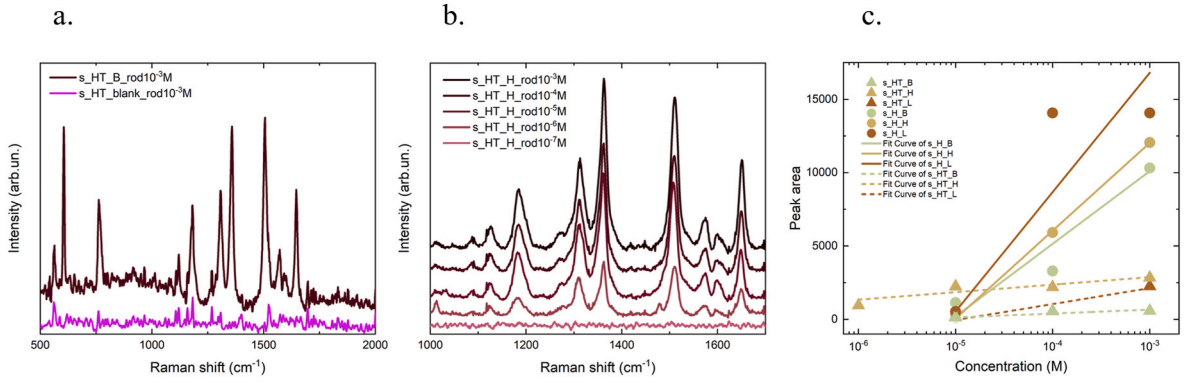

Fig. 6. (a) Comparison of Raman spectrum vs SERS spectrum of Rh6G 10^{-3} M; (b) SERS spectra of Rh6G at different concentrations (10^{-3} M – 10^{-7} M) on sample s_HT_H with 633 nm laser; (c) quantification curves obtained by plotting areas of Rh6G 1510 cm^{-1} peak at different concentrations on different substrates, calculated from curve fitting.

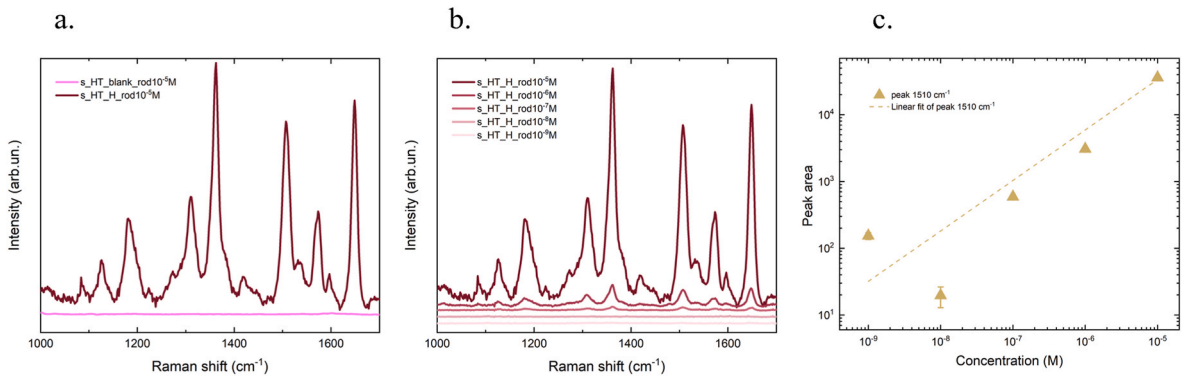

Fig. 7. (a) Comparison of Raman spectrum vs SERS spectrum of Rh6G 10^{-5} M; (b) SERS spectra of Rh6G at different concentrations (10^{-5} M – 10^{-9} M) on sample s_HT_H with 532 nm laser; (c) quantification curve obtained by plotting areas of Rh6G 1510 cm^{-1} peak, estimated from data fitting, at different concentrations.

Additionally, as observable in Fig. 6c, an exponential response between SERS signal area and the logarithm of concentration is preserved using a different laser, demonstrating the versatile application of the substrates and their use as analytical devices. The LOD threshold is indicative of high sensitivity, and it is lower or comparable to that of several different substrates published in the last decade [33,70,75–80].

3.4.2. Tests on selected analytes

After evaluating the potentiality of the substrates as a SERS platform, to further assess their versatility, three molecules – namely Malachite Green (MG), Alizarin (A) and Ochratoxin A (OTA) – were selected to test the substrate performance under different conditions and across different classes of analytes. This approach enables the characterization of the substrate's sensitivity, selectivity and the overall applicability in detecting chemically diverse targets for different fields of application.

Fig. 8a shows SERS spectra of MG solutions in water at different concentrations recorded on s_HT_H substrate in the range 700–1800 cm^{-1}. In each spectrum most of the fingerprint signal of the green dye is visible, although some changes in relative intensity and some shifts in peak position occur upon concentration. Despite these issues, the band at 1174 cm^{-1}, corresponding to the in-plane C–H bending, was selected as candidate for sensing performance quantification, since it was still visible and integrable at 10^{-9} M due to the low interference from the substrate in that region [81,82]. The observation of varying SERS spectral shapes at lower concentration is usually attributed to different orientation of the benzene ring in MG molecules when interacting with the plasmonic substrate [14,83]. For this reason, the in-plane C–C ring vibration at 1615 cm^{-1}, which is typically reported as a marker for MG detection [22,82], was not used in this study. As already mentioned elsewhere above, the SERS signal is quite sensitive to the local density of hotspots on the substrate, which can vary from point to point according to NPs distribution and size. To reduce this variability and to rule out possible interactions, we indeed analyzed the ratio between the Malachite Green (MG) peak at 1174 cm^{-1} and the substrate's peak at 763 cm^{-1} for all solutions at different MG concentration (Fig. 8b). Indeed, we observed an exponential trend by plotting the logarithm of the MG solution concentration against the ratio of the peak area at 1174 cm^{-1}, characteristic of MG, to the peak area at 763 cm^{-1}, attributed to the substrate. This approach demonstrates the sensitivity of the method, allowing for quantification of MG concentrations across a wide range.

Fig. 9a shows the spectra of A solution in ethanol recorded on s_HT_H substrate in the range 700–1800 cm^{-1}, where the characteristic peaks of anthraquinone dyes are clearly visible. Despite this, also in this case, the relative intensities vary with concentration, signals remain consistent. For instance, the peak at 1280 cm^{-1} corresponding to C–O and C–C stretching and the 1320 cm^{-1} peak attributed to C–C ring stretching show strong signals even at very low concentrations [84–86]. Moreover, the peak at 1448 cm^{-1} is associated with C–O stretching, C–H and C–O–H bending vibrations and the peaks at 1566 and 1602 cm^{-1} are due to C–C stretching [86]. The quantification curve was again constructed through normalization by calculating the ratio of the peak area at 1320 cm^{-1}, selected as a marker for A, to the peak area at 763 cm^{-1}, attributed to the blank. Although the peaks were still integrable at 10^{-10} M, the area calculated was slightly above zero, making it impossible to reliably calculate the area ratio. We report in Fig. 9b the resulting quantification curve down to 10^{-9} M which exhibits an exponential decrease proportional to the concentration.

About measurements on OTA solutions, they were performed on the

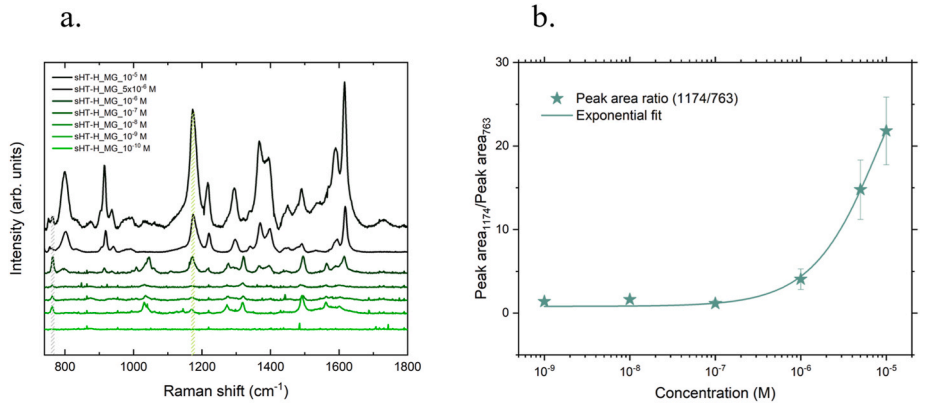

Fig. 8. (a) SERS spectra of Malachite Green acquired at different concentrations (10^{-5} M – 10^{-10} M) on sample s_HT_H with 633 nm laser. (b) quantification curve obtained by plotting the Malachite Green 1174 cm^{-1} peak area normalized to that of the substrate 763 cm^{-1} peak. Peak areas were estimated by data fitting. (For interpretation of the references to color in this figure legend, the reader is referred to the Web version of this article.)

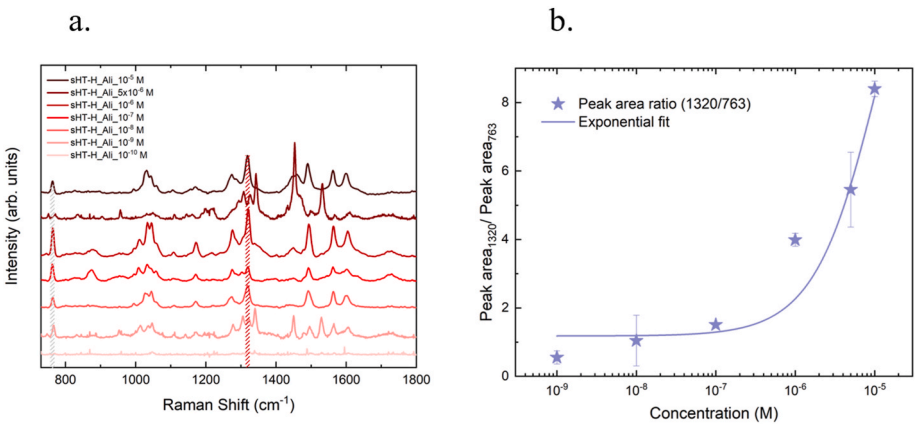

Fig. 9. (a) SERS spectra of Alizarin at different concentrations (10^{-5} M – 10^{-8} M) on sample s_HT_H with 633 nm laser; (b) quantification curve obtained by plotting the Alizarin 1320 cm^{-1} peak area normalized to that of the substrate 763 cm^{-1} peak. Peak areas were estimated by data fitting.

same substrate (sample s_HT_H) in the range between 10^{-5} M – 10^{-10} M in the range 700–1800 cm^{-1}. However, only the highest concentration of OTA was detectable in the spectra, as shown in Fig. A3 (SM), with the most intense peak, observed at 1027 cm^{-1}, attributed to in-plane C–H bending of phenylalanine [64]. Indeed, the peak typically used for the identification and quantification of this toxin, located at 1003 cm^{-1} and assigned to the ring breathing modes in the molecule [64,65], was not visible in any of the spectra. Additionally, the amide-related peak near 1600 cm^{-1} could not be utilized for quantification as it was also present in the blank spectrum.

4. Conclusions

The polymer brush-based platform, whose fabrication we reported in this paper, demonstrates a remarkable potential. Its straightforward synthetic pathway and highly customizable material properties make it a versatile and highly adaptable analytical tool. Specifically, the network organization, degree of cross-linking, and composition of the polymer brushes can be precisely tailored to meet specific application requirements. The stabilization of AgNPs provided by polymer brushes, alongside the modularity of the resulting 3D structures, sets this platform apart from traditional colloidal substrates, facilitating seamless integration into multiparameter analytical systems. Although the present study is a proof-of-concept and focuses primarily on demonstrating the platform's stability and structural versatility, a future improvement of the system may exploit NP functionalization to build sensor arrays capable of multi-analyte detection. Moreover, a more structured long-term stability study is certainly necessary. However, it falls beyond the scope of the present work, which is primarily focused on the characterization and selection of the most suitable analytical system for obtaining a reliable and measurable SERS signal. For this reason, also the assessment of selectivity was not carried out at this stage as it represents a deeper aspect which takes into account various parameters (e.g., matrix effects and measurements conditions) and would have requested more trials beyond our scope. Additionally, at this stage, we can assume that the vibrational fingerprinting capability of SERS technique enables reasonable expectation for selectivity. Indeed, we demonstrated that LSPR properties of the substrates and the possibility to perform SERS measurements ensure both high sensitivity and enable the achievement of low limits of detection, making it a powerful tool for non-target detection across various fields, including environmental monitoring and cultural heritage preservation. In particular, we demonstrated the successful identification of a variety of dyes: Rhodamine 6G – employed as a validation molecule – exhibited clear and consistent signals; Malachite Green was detectable, albeit with spectral shape variations as a function of concentration; Alizarin, despite presenting several overlapping peaks with the background, allowed for precise quantification down to low concentration. Finally, the test of detectability of Ochratoxin A was successful only at the highest concentration measured, indicating the need for further optimization in its detection. Furthermore, the possibility to integrate this technology with complementary detection systems, such as colorimetry and electrochemistry, underscores the platform as being a robust and versatile solution to address complex analytical challenges.

CRediT authorship contribution statement

Greta Peruzzi: Writing – original draft, Visualization, Validation, Investigation, Formal analysis, Data curation. **Alessandro Ciccola:** Writing – original draft, Visualization, Project administration, Investigation, Conceptualization. **Francesca Costantini:** Writing – review & editing, Methodology, Conceptualization. **Claudia Fasolato:** Writing – review & editing, Formal analysis, Data curation. **Valentina Nigro:** Writing – review & editing, Formal analysis, Data curation. **Cesare Manetti:** Supervision, Resources. **Paolo Postorino:** Supervision, Resources. **Gabriele Favero:** Supervision, Project administration, Funding acquisition.

Notes

All authors have given approval to the final version of the manuscript.

Declaration of competing interest

The authors declare that they have no known competing financial interests or personal relationships that could have appeared to influence the work reported in this paper.

Acknowledgements

This project is supported by Spoke 7 Project PE05-CHANGES-SPOKE-7-DBA CUP B53C22003780006, National Recovery and Resilience Plan (NRRP) Mission 4 Component 2 Investment 1.3, funded by the European Union–Next Generation EU.

This research was funded by the Agritech National Research Center and received funding from the European Union Next-Generation EU (PIANO NAZIONALE DI RIPRESA E RESILIENZA (PNRR) – MISSIONE 4 COMPONENTE 2, INVESTIMENTO 1.4 – D.D. 1032 June 17, 2022, CN00000022).

Appendix A. Supplementary data

Supplementary data to this article can be found online at https://doi.

org/10.1016/j.aca.2025.344653.

Data availability

Data will be made available on request.

References

[1] T.M.S. Ashrafi, G. Mohanty, Surface plasmon resonance sensors: a critical review of recent advances, market analysis, and future directions, Plasmonics (2025), https://doi.org/10.1007/s11468-024-02740-4.

[2] M. Soler, C.S. Huertas, L.M. Lechuga, Label-free plasmonic biosensors for point-of-care diagnostics: a review, Expert Rev. Mol. Diagn 19 (2019) 71–81, https://doi.org/10.1080/14737159.2019.1554435.

[3] L. Song, J. Chen, B. Bin Xu, Y. Huang, Flexible plasmonic biosensors for healthcare monitoring: progress and prospects, ACS Nano 15 (2021) 18822–18847, https://doi.org/10.1021/acsnano.1c07176.

[4] H. Yuan, G. Sun, W. Peng, W. Ji, S. Chu, Q. Liu, Y. Liang, Thymine-functionalized gold nanoparticles (Au NPs) for a highly sensitive fiber-optic surface plasmon resonance mercury ion nanosensor, Nanomaterials 11 (2021) 1–12, https://doi.org/10.3390/nano11020397.

[5] C. Genslein, P. Hausler, E.-M. Kirchner, R. Bierl, A.J. Baeumner, T. Hirsch, Graphene-enhanced plasmonic nanohole arrays for environmental sensing in aqueous samples, Beilstein J. Nanotechnol. 7 (2016) 1564–1573, https://doi.org/10.3762/bjnano.7.150.

[6] S. Balbinot, A.M. Srivastav, J. Vidic, I. Abdulhalim, M. Manzano, Plasmonic biosensors for food control, Trends Food Sci. Technol. 111 (2021) 128–140, https://doi.org/10.1016/j.tifs.2021.02.057.

[7] L.A. Putri, Y.D. Prabowo, D.M.M. Dewi, Z. Mumtazah, F.P. Adila, G. Fadillah, T. Amrillah, K. Triyana, F.A.A. Nugroho, H.S. Wasisto, Review of noble metal nanoparticle-based colorimetric sensors for food safety monitoring, ACS Appl. Nano Mater. 7 (2024) 19821–19853, https://doi.org/10.1021/acsanm.4c04327.

[8] Z. Li, Z. Wang, J. Khan, M.K. Lagasse, K.S. Suslick, Ultrasensitive monitoring of museum airborne pollutants using a silver nanoparticle sensor array, ACS Sens. 5 (2020) 2783–2791, https://doi.org/10.1021/acssensors.0c00583.

[9] N. La Ngoc Tran, T.A. Nguyen, T. Le Hoang Doan, H.V.T. Nguyen, V.T. Huong, T. T. Van Tran, H. Ju, T.H. Huy, H. Van Le, N.H.T. Tran, Stacking-order reversed multilayers of ZIF-8 and silver nanoparticles for the SERS detection of organic dye species, ChemNanoMat 9 (2023), https://doi.org/10.1002/cnma.202300164.

[10] J. Hodgkinson, R.P. Tatam, Optical gas sensing: a review, Meas. Sci. Technol. 24 (2013), https://doi.org/10.1088/0957-0233/24/1/012004.

[11] O. Stranik, R. Nooney, C. McDonagh, B.D. MacCraith, Optimization of nanoparticle size for plasmonic enhancement of fluorescence, Plasmonics 2 (2007) 15–22, https://doi.org/10.1007/s11468-006-9020-9.

[12] M. Bauch, K. Toma, M. Toma, Q. Zhang, J. Dostalek, Plasmon-enhanced fluorescence biosensors: a review, Plasmonics 9 (2014) 781–799, https://doi.org/10.1007/s11468-013-9660-5.

[13] Z. Wu, J. Li, T. Zhang, K. Zhang, X. Liu, Z. Yang, L. Xu, K. Han, One-pot synthesized three-way junction based multiple strand displacement amplification for sensitive assay of H5N1 DNA, Analyst 150 (2025) 1541–1552, https://doi.org/10.1039/d4an01586j.

[14] S. Schlücker, Surface-enhanced raman spectroscopy: concepts and chemical applications, Angew. Chem., Int. Ed. 53 (2014) 4756–4795, https://doi.org/10.1002/anie.201205748.

[15] F. Pozzi, M. Leona, Surface-enhanced Raman spectroscopy in art and archaeology, J. Raman Spectrosc. 47 (2016) 67–77, https://doi.org/10.1002/jrs.4827.

[16] R.A. Halvorson, P.J. Vikesland, Surface-enhanced raman spectroscopy (SERS) for environmental analyses, Environ. Sci. Technol. 44 (2010) 7749–7755, https://doi.org/10.1021/es101228z.

[17] M.F. Cardinal, E. Vander Ende, R.A. Hackler, M.O. McAnally, P.C. Stair, G. C. Schatz, R.P. Van Duyne, Expanding applications of SERS through versatile nanomaterials engineering, Chem. Soc. Rev. 46 (2017) 3886–3903, https://doi.org/10.1039/C7CS00207F.

[18] L. Jiang, M.M. Hassan, S. Ali, H. Li, R. Sheng, Q. Chen, Evolving trends in SERS-based techniques for food quality and safety: a review, Trends Food Sci. Technol. 112 (2021) 225–240, https://doi.org/10.1016/j.tifs.2021.04.006.

[19] M. Kahraman, E.R. Mullen, A. Korkmaz, S. Wachsmann-Hogiu, Fundamentals and applications of SERS-based bioanalytical sensing, Nanophotonics 6 (2017) 831–852, https://doi.org/10.1515/nanoph-2016-0174.

[20] K.C. Bantz, H.D. Nelson, C.L. Haynes, Plasmon-enabled study of self-assembled alkanethiol ordering on roughened Ag substrates, J. Phys. Chem. C 116 (2012) 3585–3593, https://doi.org/10.1021/jp2098334.

[21] Y. ning Liu, J. jun Li, G. jun Weng, J. Zhu, J. wu Zhao, Reliable detection of malachite green by self-assembled SERS substrates based on gold–silicon heterogeneous nano pineapple structures, Food Chem. 451 (2024), https://doi.org/10.1016/j.foodchem.2024.139454.

[22] H.M. Saleh, T. El-Brolossy, T. Sharaf, H. Talaat, SERS substrates for ultrasensitive detection of malachite green using silver nanostars, J. Appl. Spectrosc. (2025), https://doi.org/10.1007/s10812-025-01859-4.

[23] M.V. Simas, P.O. Olaniyan, S. Hati, G.A. Davis, G. Anspach, J.V. Goodpaster, N. E. Manicke, R. Sardar, Superhydrophobic surface modification of polymer microneedles enables fabrication of multimodal surface-enhanced raman spectroscopy and mass spectrometry substrates for synthetic drug detection in blood plasma, ACS Appl. Mater. Interfaces 15 (2023) 46681–46696, https://doi.org/10.1021/acsami.3c10174.

[24] W. Shang, H. Xin, X. Hou, L. Wu, L. Wu, Multifunctional SERS substrate for simultaneous detection of multiple contaminants and photothermal removal of pathogenic bacteria, ACS Appl. Mater. Interfaces (2024), https://doi.org/10.1021/acsami.4c10473.

[25] N. Alayo, A. Conde-Rubio, J. Bausells, X. Borrisé, A. Labarta, X. Batlle, F. Pérez-Murano, Nanoparticles with tunable shape and composition fabricated by nanoimprint lithography, Nanotechnology 26 (2015), https://doi.org/10.1088/0957-4484/26/44/445302.

[26] P. Colson, C. Henrist, R. Cloots, Nanosphere lithography: a powerful method for the controlled manufacturing of nanomaterials, J. Nanomater. 2013 (2013), https://doi.org/10.1155/2013/948510.

[27] Y. Shin, I. Jeon, Y. You, G. Song, T.K. Lee, J. Oh, C. Son, D. Baek, D. Kim, H. Cho, H. Hwang, T. Kim, S.K. Kwak, J. Kim, J. Lee, Facile microfluidic fabrication of 3D hydrogel SERS substrate with high reusability and reproducibility via programmable maskless flow microlithography, Adv. Opt. Mater. 8 (2020), https://doi.org/10.1002/adom.202001586.

[28] Y. Song, H.E. Elsayed-Ali, Aqueous phase Ag nanoparticles with controlled shapes fabricated by a modified nanosphere lithography and their optical properties, Appl. Surf. Sci. 256 (2010) 5961–5967, https://doi.org/10.1016/j.apsusc.2010.03.102.

[29] M. Blanco-Formoso, N. Pazos-Perez, R.A. Alvarez-Puebla, Fabrication of plasmonic supercrystals and their SERS enhancing properties, ACS Omega 5 (2020) 25485–25492, https://doi.org/10.1021/acsomega.0c03412.

[30] M. Alba, N. Pazos-Perez, B. Vaz, P. Formentin, M. Tebbe, M.A. Correa-Duarte, P. Granero, J. Ferré-Borrull, R. Alvarez, J. Pallares, A. Fery, A.R. De Lera, L. F. Marsal, R.A. Alvarez-Puebla, Macroscale plasmonic substrates for highly sensitive surface-enhanced raman scattering, Angew. Chem., Int. Ed. 52 (2013) 6459–6463, https://doi.org/10.1002/anie.201302285.

[31] Y. Du, L. Shi, T. He, X. Sun, Y. Mo, SERS enhancement dependence on the diameter and aspect ratio of silver-nanowire array fabricated by anodic aluminium oxide template, Appl. Surf. Sci. 255 (2008) 1901–1905, https://doi.org/10.1016/j.apsusc.2008.06.140.

[32] J. Peng, Y. Song, Y. Lin, Z. Huang, Introduction and development of surface-enhanced raman scattering (SERS) substrates: a review, Nanomaterials 14 (2024), https://doi.org/10.3390/nano14201648.

[33] W. Sheng, W. Li, D. Tan, P. Zhang, E. Zhang, E. Sheremet, B.V.K.J. Schmidt, X. Feng, R.D. Rodriguez, R. Jordan, I. Amin, Polymer brushes on graphitic carbon nitride for patterning and as a SERS active sensing layer via incorporated nanoparticles, ACS Appl. Mater. Interfaces 12 (2020) 9797–9805, https://doi.org/10.1021/acsami.9b21984.

[34] N. Leopold, B. Lendl, A new method for fast preparation of highly surface-enhanced raman scattering (SERS) active silver colloids at room temperature by reduction of silver nitrate with hydroxylamine hydrochloride, J. Phys. Chem. B 107 (2003) 5723–5727, https://doi.org/10.1021/jp027460u.

[35] P.C. Lee, D. Melsel, Adsorption and surface-enhanced raman of dyes on silver and gold Sols1. https://pubs.acs.org/sharingguidelines, 1982.

[36] K. Mavani, M. Shah, Synthesis of silver nanoparticles by using sodium borohydride as a reducing agent, n.d. www.ijert.org.

[37] U.T. Khatoon, A. Velidandi, G.V.S. Nageswara Rao, Sodium borohydride mediated synthesis of nano-sized silver particles: their characterization, anti-microbial and cytotoxicity studies, Mater. Chem. Phys. 294 (2023), https://doi.org/10.1016/j.matchemphys.2022.126997.

[38] C. Fasolato, F. Domenici, S. Sennato, F. Mura, L. De Angelis, F. Luongo, F. Costantini, F. Bordi, P. Postorino, Dimensional scale effects on surface enhanced Raman scattering efficiency of self-assembled silver nanoparticle clusters, Appl. Phys. Lett. 105 (2014), https://doi.org/10.1063/1.4893373.

[39] Q. Zhang, X.D. Wang, T. Tian, L.Q. Chu, Incorporation of multilayered silver nanoparticles into polymer brushes as 3-dimensional SERS substrates and their application for bacteria detection, Appl. Surf. Sci. 407 (2017) 185–191, https://doi.org/10.1016/j.apsusc.2017.02.202.

[40] L. Cong, X. Wang, J. Wang, W. Liu, W. Xu, S. Zhang, S. Xu, Three-dimensional SERS-active hydrogel microbeads enable highly sensitive homogeneous phase detection of alkaline phosphatase in biosystems, ACS Appl. Mater. Interfaces (2025), https://doi.org/10.1021/acsami.4c18139.

[41] J. Song, G. Huang, F. Wei, J. Meng, K. Zhang, High-performance flexible strain sensors: the role of In-Situ cross-linking and interface engineering in liquid metal-carbon Nanotube-PDMS composites, ACS Appl. Mater. Interfaces (2024), https://doi.org/10.1021/acsami.4c17983.

[42] K.O. Hukum, T. Caykara, G. Demirel, Thermoresponsive polymer brush-decorated 3-D plasmonic gold nanorod arrays as an effective plasmonic sensing platform, ACS Appl. Polym. Mater. 5 (2023) 4296–4304, https://doi.org/10.1021/acsapm.3c00466.

[43] X. Li, X. Li, W. Wang, Grafting PDMAEMA brushes onto graphene oxide for fabricating Ag nanosheet-assembled microspheres as SERS substrates, Chem. Phys. Lett. 813 (2023), https://doi.org/10.1016/j.cplett.2023.140296.

[44] C.J. Porter, J.R. Werber, C.L. Ritt, Y.F. Guan, M. Zhong, M. Elimelech, Controlled grafting of polymer brush layers from porous cellulosic membranes, J.Memb. Sci. 596 (2020), https://doi.org/10.1016/j.memsci.2019.117719.

[45] Q. Zhang, J.J. Yin, F. Liu, X.N. Zou, L.Q. Chu, Immobilization of silver nanoparticles into POEGMA polymer brushes as SERS-active substrates, Surf. Interface Anal. 49 (2017) 316–322, https://doi.org/10.1002/sia.6137.

[46] B. Zhao, W.J. Brittain, Polymer brushes: surface-immobilized macromolecules, Prog. Polym. Sci. 25 (2000) 677–710, https://doi.org/10.1016/S0079-6700(00)00012-5.

[47] J. Song, B. Duan, C. Wang, J. Zhou, L. Pu, Z. Fang, P. Wang, T.T. Lim, H. Duan, SERS-encoded nanogapped plasmonic nanoparticles: growth of metallic nanoshell by templating redox-active polymer brushes, J. Am. Chem. Soc. 136 (2014) 6838–6841, https://doi.org/10.1021/ja502024d.
[48] D.-Y. Wang, T.-S. Teng, Y.-C. Wu, Y.-C. Lee, K.-H. Chen, C.-H. Chen, Y.-C. Chang, C.-C. Chen, Silver-nanoparticle-conjugated polypeptide brushes for surface-enhanced raman scattering, J. Phys. Chem. C 113 (2009) 13498–13504, https://doi.org/10.1021/jp903664u.
[49] A. Murad Bhayo, Y. Yang, X. He, Polymer brushes: synthesis, characterization, properties and applications, Prog. Mater. Sci. 130 (2022) 101000, https://doi.org/10.1016/j.pmatsci.2022.101000.
[50] S. Gupta, M. Agrawal, M. Conrad, N.A. Hutter, P. Olk, F. Simon, L.M. Eng, M. Stamm, R. Jordan, Poly(2-(dimethylamino)ethyl methacrylate) brushes with incorporated nanoparticles as a SERS active sensing layer, Adv. Funct. Mater. 20 (2010) 1756–1761, https://doi.org/10.1002/adfm.201000025.
[51] O. Azzaroni, Polymer brushes here, there, and everywhere: recent advances in their practical applications and emerging opportunities in multiple research fields, J. Polym. Sci. Polym. Chem. 50 (2012) 3225–3258, https://doi.org/10.1002/pola.26119.
[52] L. Xu, Z. Chu, J. Zhang, T. Cai, X. Zhang, Y. Li, H. Wang, X. Shen, R. Cai, H. Shi, C. Zhu, J. Pan, D. Pan, Steric effects in the deposition mode and drug-delivering efficiency of nanocapsule-based multilayer films, ACS Omega 7 (2022) 30321–30332, https://doi.org/10.1021/acsomega.2c03591.
[53] L. Xu, X. Zhang, Z. Chu, H. Wang, Y. Li, X. Shen, L. Cai, H. Shi, C. Zhu, J. Pan, D. Pan, Temperature-responsive multilayer films based on block copolymer-coated silica nanoparticles for long-term release of favipiravir, ACS Appl. Nano Mater. 4 (2021) 14014–14025, https://doi.org/10.1021/acsanm.1c03334.
[54] L. Xu, H. Wang, Z. Chu, L. Cai, H. Shi, C. Zhu, D. Pan, J. Pan, X. Fei, Y. Lei, Temperature-responsive multilayer films of micelle-based composites for controlled release of a third-generation EGFR inhibitor, ACS Appl. Polym. Mater. 2 (2020) 741–750, https://doi.org/10.1021/acsapm.9b01051.
[55] E.M. Benetti, X. Sui, S. Zapotoczny, G. Julius Vancso, Surface-grafted gel-brush/metal nanoparticle hybrids, Adv. Funct. Mater. 20 (2010) 939–944, https://doi.org/10.1002/adfm.200902114.
[56] F. Costantini, E.M. Benetti, R.M. Tiggelaar, H.J.G.E. Gardeniers, D.N. Reinhoudt, J. Huskens, G.J. Vancso, W. Verboom, A brush-gel/metal-nanoparticle hybrid film as an efficient supported catalyst in glass microreactors, Chem. Eur J. 16 (2010) 12406–12411, https://doi.org/10.1002/chem.201000948.
[57] J. Sundaram, B. Park, Y. Kwon, Stable silver/biopolymer hybrid plasmonic nanostructures for high performance surface enhanced raman scattering (SERS), J. Nanosci. Nanotechnol. 13 (2013) 5382–5390, https://doi.org/10.1166/jnn.2013.7737.
[58] T. Chen, L. Zhao, Z. Wang, J. Zhao, Y. Li, H. Long, D. Yu, X. Wu, H. Yang, Hierarchical surface inspired by geminized cationic amphiphilic polymer brushes for super-antibacterial and self-cleaning properties, Biomacromolecules 21 (2020) 5213–5221, https://doi.org/10.1021/acs.biomac.0c01295.
[59] R. Wang, Q. Wei, W. Sheng, B. Yu, F. Zhou, B. Li, Driving polymer brushes from synthesis to functioning, Angew. Chem., Int. Ed. 62 (2023), https://doi.org/10.1002/anie.202219312.
[60] G. Mustafa, A. Hassan, M. Shahid, A. Irfan, A.R. Chaudhry, Z.H. Farooqi, R. Begum, 2-Hydroxyethyl methacrylate based polymer microgels and their hybrids, React. Funct. Polym. 200 (2024), https://doi.org/10.1016/j.reactfunctpolym.2024.105919.
[61] Z.H. Li, J.H. Bai, X. Zhang, J.M. Lv, C.S. Fan, Y.M. Zhao, Z.L. Wu, H.J. Xu, Facile synthesis of Au nanoparticle-coated Fe3O4 magnetic composite nanospheres and their application in SERS detection of malachite green, Spectrochim. Acta Mol. Biomol. Spectrosc. 241 (2020), https://doi.org/10.1016/j.saa.2020.118532.
[62] V. Daniels, T. Devièse, M. Hacke, C. Higgitt, Technological Insights into Madder Pigment Production in Antiquity, 2014.
[63] D. Cardon, Natural Dyes. Source, Tradition, Technology and Science, 2007.
[64] L.M. Rojas, Y. Qu, L. He, A facile solvent extraction method facilitating surface-enhanced Raman spectroscopic detection of ochratoxin A in wine and wheat, Talanta 224 (2021), https://doi.org/10.1016/j.talanta.2020.121792.
[65] S. Rostami, K. Zór, D.S. Zhai, M. Viehrig, L. Morelli, A. Mehdinia, J. Smedsgaard, T. Rindzevicius, A. Boisen, High-throughput label-free detection of Ochratoxin A in wine using supported liquid membrane extraction and Ag-capped silicon nanopillar SERS substrates, Food Control 113 (2020) 107183, https://doi.org/10.1016/j.foodcont.2020.107183.
[66] M. Husseman, E.E. Malmström, M. McNamara, M. Mate, D. Mecerreyes, D. G. Benoit, J.L. Hedrick, P. Mansky, E. Huang, T.P. Russell, C.J. Hawker, Controlled synthesis of polymer brushes by "Living" free radical polymerization techniques, Macromolecules 32 (1999) 1424–1431, https://doi.org/10.1021/ma981290v.
[67] M. Ider, K. Abderrafi, A. Eddahbi, S. Ouaskit, A. Kassiba, Silver metallic nanoparticles with surface plasmon resonance: synthesis and characterizations, J clust, Sci 28 (2017) 1051–1069, https://doi.org/10.1007/s10876-016-1080-1.
[68] S. Christau, T. Möller, Z. Yenice, J. Genzer, R. von Klitzing, Brush/gold nanoparticle hybrids: effect of grafting density on the particle uptake and distribution within weak polyelectrolyte brushes, Langmuir 30 (2014) 13033–13041, https://doi.org/10.1021/la503432x.
[69] P.H. Wang, T.L. Wang, W.C. Lin, H.Y. Lin, M.H. Lee, C.H. Yang, Crosslinked polymer ionic liquid/ionic liquid blends prepared by photopolymerization as solid-state electrolytes in supercapacitors, Nanomaterials 8 (2018), https://doi.org/10.3390/nano8040225.
[70] H.S.S. Sharma, E. Carmichael, D. McCall, Fabrication of SERS substrate for the detection of rhodamine 6G, glyphosate, melamine and salicylic acid, Vib. Spectrosc. 83 (2016) 159–169, https://doi.org/10.1016/j.vibspec.2016.01.011.
[71] M. Barzan, F. Hajiesmaeilbaigi, Investigation the concentration effect on the absorption and fluorescence properties of rhodamine 6G dye, Optik 159 (2018) 157–161, https://doi.org/10.1016/j.ijleo.2018.01.075.
[72] S. Liu, S. Wan, M. Chen, M. Sun, Theoretical study on SERRS of rhodamine 6G adsorbed on Ag_2 cluster: chemical mechanism via intermolecular or intramolecular charge transfer, J. Raman Spectrosc. 39 (2008) 1170–1177, https://doi.org/10.1002/jrs.1958.
[73] H. Watanabe, N. Hayazawa, Y. Inouye, S. Kawata, DFT vibrational calculations of rhodamine 6G adsorbed on silver: analysis of tip-enhanced Raman spectroscopy, J. Phys. Chem. B 109 (2005) 5012–5020, https://doi.org/10.1021/jp045771u.
[74] F. Benz, R. Chikkaraddy, A. Salmon, H. Ohadi, B. De Nijs, J. Mertens, C. Carnegie, R.W. Bowman, J.J. Baumberg, SERS of individual nanoparticles on a mirror: size does matter, but so does shape, J. Phys. Chem. Lett. 7 (2016) 2264–2269, https://doi.org/10.1021/acs.jpclett.6b00986.
[75] W. Zhang, B. Li, L. Chen, Y. Wang, D. Gao, X. Ma, A. Wu, Brushing, a simple way to fabricate SERS active paper substrates, Anal. Methods 6 (2014) 2066–2071, https://doi.org/10.1039/C4AY00046C.
[76] S. Lin, W.-L.-J. Hasi, X. Lin, S. Han, X.-T. Lou, F. Yang, D.-Y. Lin, Z.-W. Lu, Rapid and sensitive SERS method for determination of Rhodamine B in chili powder with paper-based substrates, Anal. Methods 7 (2015) 5289–5294, https://doi.org/10.1039/C5AY00028A.
[77] N.T.T. Phuong, T.-A. Nguyen, V.T. Huong, L.H. Tho, D.T. Anh, H.K.T. Ta, T.H. Huy, K.T.L. Trinh, N.H.T. Tran, Sensors for detection of the synthetic dye rhodamine in environmental monitoring based on SERS, Micromachines (Basel) 13 (2022) 1840, https://doi.org/10.3390/mi13111840.
[78] G.A. Khan, Ö. Demirtaş, A.K. Demir, Ö. Aytekin, A. Bek, A.S. Bhatti, W. Ahmed, Fabrication of flexible, cost-effective, and scalable silver substrates for efficient surface enhanced Raman spectroscopy based trace detection, Colloids Surf. A Physicochem. Eng. Asp. 619 (2021), https://doi.org/10.1016/j.colsurfa.2021.126542.
[79] S. Mao, F. Pei, S. Feng, Q. Hao, P. Zhang, Z. Tong, X. Mu, W. Lei, B. Liu, Detection of trace Rhodamine B using stable, uniformity, and reusable SERS substrate based on Ag@SiO2-Au nanoparticles, Colloids Surf. A Physicochem. Eng. Asp. 657 (2023) 130595, https://doi.org/10.1016/j.colsurfa.2022.130595.
[80] N. Tran Truc Phuong, T. Xoan Hoang, N. La Ngoc Tran, L. Gia Phuc, V.-D. Phung, H. Kieu Thi Ta, T. Ngoc Bach, N. Hoa Thi Tran, K. The Loan Trinh, Rapid and sensitive detection of Rhodamine B in food using the plasmonic silver nanocube-based sensor as SERS active substrate, Spectrochim. Acta Mol. Biomol. Spectrosc. 263 (2021) 120179, https://doi.org/10.1016/j.saa.2021.120179.
[81] K. Sivashanmugan, J.-D. Liao, B.H. Liu, C.-K. Yao, S.-C. Luo, Ag nanoclusters on ZnO nanodome array as hybrid SERS-active substrate for trace detection of malachite green, Sensor. Actuator. B Chem. 207 (2015) 430–436, https://doi.org/10.1016/j.snb.2014.10.088.
[82] T.T.K. Chi, N.T. Le, B.T.T. Hien, D.Q. Trung, N.Q. Liem, Preparation of SERS substrates for the detection of organic molecules at low concentration, Commun. Phys. 26 (2017) 261, https://doi.org/10.15625/0868-3166/26/3/8053.
[83] P. Kumar, R. Khosla, M. Soni, D. Deva, S.K. Sharma, A highly sensitive, flexible SERS sensor for malachite green detection based on Ag decorated microstructured PDMS substrate fabricated from Taro leaf as template, Sensor. Actuator. B Chem. 246 (2017) 477–486, https://doi.org/10.1016/j.snb.2017.01.202.
[84] A.V. Whitney, R.P. Van Duyne, F. Casadio, An innovative surface-enhanced Raman spectroscopy (SERS) method for the identification of six historical red lakes and dyestuffs, in: Journal of Raman Spectroscopy, John Wiley and Sons Ltd, 2006, pp. 993–1002, https://doi.org/10.1002/jrs.1576.
[85] S. Bruni, V. Guglielmi, F. Pozzi, Historical organic dyes: a surface-enhanced Raman scattering (SERS) spectral database on Ag Lee-Meisel colloids aggregated by NaClO4, J. Raman Spectrosc. 42 (2011) 1267–1281, https://doi.org/10.1002/jrs.2872.
[86] M.V. Cañamares, J.V. Garcia-Ramos, C. Domingo, S. Sanchez-Cortes, Surface-enhanced Raman scattering study of the adsorption of the anthraquinone pigment alizarin on Ag nanoparticles, J. Raman Spectrosc. 35 (2004) 921–927, https://doi.org/10.1002/jrs.1228.